A. Yamanaka, T. Takaki and Y. Tomita / Proceedings, AES – ATEMA' 2007 International Conference, Montreal, Canada, August 06 -10, 2007, pp. 213 - 221

ISBN 0-9780479

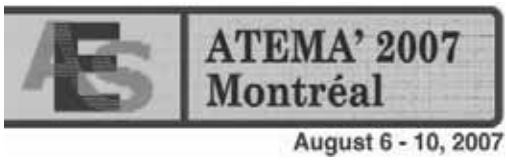

International Conference on Advances and Trends in Engineering Materials and their Applications (AES – ATEMA' 2007)

Numerical Modeling of Microstructural Formation and Deformation Behavior of Fe-C Alloy

A. Yamanaka [1]*, T. Takaki [2] and Y. Tomita [3]

[1]Graduate School of Science and Technology, Kobe University, 1-1, Rokko-dai, Nada, Kobe, Hyogo, 657-8501, Japan
(Email: yamanaka@solid.mech.kobe-u.ac.jp)

[2]Faculty of Maritime Sciences, Kobe University, 5-1-1, Fukaeminami, Higashinada, Kobe, Hyogo, 658-0022, Japan
(Email: takaki@maritime.kobe-u.ac.jp)

[3]Faculty of Engineering, Kobe University, 1-1, Rokko-dai, Nada, Kobe, Hyogo, 657-8501, Japan
(Email: tomita@mech.kobe-u.ac.jp)

*Corresponding Author

Abstract

We develop a numerical model for the prediction of the microstructure formation and deformation behaviour of an Fe-C alloy by coupling the phase-field (PF) method with the finite element method based on the homogenization method (FEH). The PF simulation clarifies the growth of the ferrite phase during the γ/α transformation in the Fe-C alloy. The FEH analysis employs the morphology of the α phase and is used to evaluate the mechanical properties of the Fe-C alloy. Furthermore, the FEH analysis is performed to investigate the effects of the configuration of microstructures on the deformation behaviour. The results show that the deformation behaviour dependence on the morphology of the α phase is quantitatively in agreement with experimental results. This study suggests the applicability of the proposed model, which enables us to systematically evaluate the mechanical properties of the Fe-C alloy accompanying with the morphological change of the microstructures.

Keywords

Phase-Field Method, Homogenization Method, Fe-C alloy, Numerical Simulation.

1 Introduction

The mechanical properties of steels, such as tensile strength, ductility and toughness, are related to their inhomogeneous microscopic deformation behaviour. The deformation behaviour in the microscopic region is largely characterized not only by that volume fraction of the constituent phases, but also the morphology of the microstructure that is formed during phase transformations or precipitation. For simple carbon steel or an Fe-C alloy, it is well known that the microstructure can consist of any of the austenite, ferrite, pearlite, bainite and martensite. These component microstructures exhibit various morphologies and affect the mechanical behaviour [1]. For example, in the ferrite-pearlite steel, the configuration of a softer ferrite (α) phase strongly influences the ductility and toughness of the steel. Because of the above reasons, to efficiently control the mechanical properties of steels or alloys, it is essential to develop a numerical model to predict the microstructural formation and systematically clarify the relationship between the morphology of the microstructure and the micro- and macroscale deformation behaviour.

Time-dependent Ginzburg-Landau (TDGL) theory and phase-field (PF) theory have been proposed as powerful tools for the prediction of microstructural evolution [2]. The PF approach has an advantage that it can simulate the evolution of microstructures without explicit tracking of the position of the interface. Furthermore, in terms of the evaluation of the mechanical properties of materials, the two-scale finite element method using homogenization theory (FEH) has attracted attention as an excellent numerical technique for the investigation of the micro- and macroscopic deformation behaviour of materials [3, 4]. These numerical models have been applied to Fe-based alloys. However, according to the author's knowledge, there has been no integrated numerical study using both the PF method and FEH analysis for the microstructure and mechanical modelling of Fe-based alloys.

In the present study, the main purpose is to develop an integrated numerical model for the microstructure design of the Fe-C alloy by coupling the PF method with FEH analysis. Using our proposed simulation model, we systematically investigate the mechanical properties of the Fe-C alloy taking into account the morphological change of the microstructure. We first simulate the evolution of the α phase due to the austenite-to-ferrite (γ/α) transformation below the Ae3 temperature by the PF method. Then, elastic-plastic FEH analysis is performed using an unit-cell that represents the simulated microstructure in the PF simulation. Through this procedure, we investigate the distribution of the internal stress-strain field in the microstructure and the effects of the morphological change of the α phase on the mechanical properties of the Fe-C alloy.

2 Phase-Field Method of the Austenite to Ferrite Transformation in Fe-C Alloy

For the formation of the microstructure in the Fe-C alloy, the authors proposed the PF model for the γ/α transformation and the morphological change of the ferrite phase [5]. The PF model for the γ/α transformation is summarized below.

The TDGL equation, which describes the evolution of microstructure during the γ/α transformation, is derived by assuming that the

total free energy of the Fe-C alloy decreases monotonically with time. The total free energy of the Fe-C alloy is defined by the Ginzburg-Landau-type Gibbs free energy functional as follows:

$$G = \int_V \left\{ g(\phi, u_C, T) + \frac{\varepsilon^2(\theta)}{2} |\nabla \phi|^2 \right\} dV , \quad (1)$$

where the first and second terms of Eqn.(1) are the chemical free energy density and the gradient energy density, respectively. Here, ϕ is the nonconserved order parameter, phase field, defined as $\phi = 1$ in the α phase and $\phi = 0$ in the austenite phase. u_C is the carbon concentration related to the normal mole fraction of a carbon atom. T denotes temperature.

The chemical free energy density of the Fe-C alloy is postulated to be of the following form.

$$g(\phi, u_C, T) = p(\phi) g^{\alpha}(u_C, T) + (1 - p(\phi)) g^{\gamma}(u_C, T) + W q(\phi) \quad (2)$$

Here, $g^{\alpha}(u_C, T)$ and $g^{\gamma}(u_C, T)$ are the chemical free energy densities of the pure α phase and pure austenite phase, respectively. These chemical free energy densities are obtained from the literature [6]. Also, $p(\phi) = \phi^2 (10\text{-}15\,\phi + 6\,\phi^2)$, $q(\phi) = \phi^2 (1 - \phi)^2$ and W are the free energy density function, the double-well potential function and the height of the potential, respectively. In the gradient term of the total free energy, $\varepsilon(\theta)$ is the gradient energy coefficient, which describes the interfacial anisotropy and is related to the interfacial energy σ and the interfacial thickness δ as follows.

$$\varepsilon(\theta) = \sqrt{\frac{3\sigma\delta}{b}} \{1 + \xi \cos k(\theta - \theta_0)\} \equiv \bar{\varepsilon}(\theta) \quad (3)$$

Here, ξ, k, θ and θ_0 are the strength of the anisotropy, the mode number of the anisotropy, the angle between the interfacial normal and the x-axis and the preferential growth orientation, respectively. In this study, we employ the following regularized gradient energy coefficient in the case of a high interfacial anisotropy such as $\xi > 1/(k^2\text{-}1)$ [7]:

$$\varepsilon(\theta) = \begin{cases} \sqrt{\frac{3\sigma\delta}{b}} \{1 + \xi \cos k(\theta - \theta_0)\} \\ (for \quad 2\pi i/k + \theta_m \le \theta - \theta_0 \le 2\pi(i+1)/k + \theta_m) \\ \frac{\bar{\varepsilon}(\theta_m + \theta_0)}{\cos\theta_m} \cos(\theta - \theta_0) \\ (for \quad 2\pi i/k - \theta_m \le \theta - \theta_0 \le 2\pi i/k + \theta_m) \end{cases} . \quad (4)$$

Here, θ_{m} is defined as the first missing orientation.

The governing equations for the phase field ϕ and the carbon concentration u_{C} are derived from the TDGL equations using the total free energy of the Fe-C alloy as follows:

$$\frac{\partial \phi}{\partial t} = M_{\phi} \left[\nabla \cdot \left\{ \varepsilon(\theta)^2 \nabla \phi \right\} - \frac{\partial g}{\partial \phi} - \frac{\partial}{\partial x} \left\{ \varepsilon(\theta) \frac{\partial \varepsilon}{\partial x} \frac{\partial \phi}{\partial y} \right\} + \frac{\partial}{\partial y} \left\{ \varepsilon(\theta) \frac{\partial \varepsilon}{\partial y} \frac{\partial \phi}{\partial x} \right\} \right] \quad (5)$$

and

$$\frac{\partial u_C}{\partial t} = \nabla \cdot \left[D_C(u_C, T) \left\{ \frac{\partial^2 g}{\partial {u_C}^2} \nabla u_C + \frac{\partial^2 g}{\partial u_C \partial \phi} \nabla \phi \right\} \right], \quad (6)$$

where M_{ϕ} is the kinetic parameter for ϕ, which is related to the mobility of the α/ γ interface $M_{\alpha/\gamma}$ as [8]:

$$M_{\phi} = M_{\alpha/\gamma} \frac{\sqrt{2W}}{6\varepsilon_0} . \quad (7)$$

$D_C(u_C, T)$ is the parameter for the carbon concentration, which is related to $p(\phi)$ and the concentration- and temperature-dependent mobilities of the carbon atoms in the constituent phases as follows [9, 10]:

$$D_C(u_C, T) = v_m u_c \left\{ p(\phi) \left(1 - \frac{u_C}{3} \right) + (1 - p(\phi))(1 - u_C) \right\} \times M_C^{\alpha\, p(\phi)} M_C^{\gamma\, 1 - p(\phi)} . \quad (8)$$

3 Finite Element Method Based on the Two-Scale Homogenization Method

In order to investigate the deformation

properties of the Fe-C alloy foe different microstructures, large-deformation FEH analysis is performed in two-dimensions. In this analysis, we consider the Fe-C alloy as a ferrite-pearlite two-phase alloy. The microscale distribution of the constituent phases in the steel is determined from the PF simulations and is described using the unit-cell, as mentioned in the following section.

The Fe-C alloy is considered to be an isotropic elastic-plastic material and its deformation behavior is characterized by J_2 flow theory. Therefore, we employ the Plandtl-Reuss equation as the constitutive equation, that is, the relationship between the Jaumann rate of the Kirchhoff stress $\overset{\nabla}{S}_{ij}$ and the strain rate $\dot{\varepsilon}_{ij}$ [11]:

$$\overset{\nabla}{S}_{ij} = \left\{ D^{e}_{ijkl} - \frac{3G\sigma'_{ij}\sigma'_{kl}}{\sigma^{2}_{eq}\left(H'/3G+1\right)} \right\} \dot{\varepsilon}_{kl}, \qquad (9)$$

where D^{e}_{ijkl}, σ'_{ij} and σ_{eq} are the elastic coefficient matrix, the deviatric stress tensor and the equivalent stress, respectively. H' is the plastic tangent modulus. Using this constitutive equation, we solve the two-scale elastic-plastic boundary value problem by the FEH method [4].

4 Computational Model

Figure 1 (a) shows the computational model, initial condition and boundary condition for the PF simulation. The size of the computational domain is 5 × 6 μm^2 and the zero Neumann boundary condition is employed. In the PF simulation, we simulate the evolution and morphological change of the preexisting α phase at the austenite grain boundary, i.e., the grain boundary allotriomorph ferrite (α_A). Therefore, assuming that the α_A is nucleated at the hexagonal austenite grain boundary, we set the initial α phase in the computational domain. The initial concentration is supersaturated in the austenite matrix and at equilibrium in the α phase. Since we simulate the isothermal transformation, the temperature is set to be constant at T = 1000 K. Although the growth direction of the α phase depends on the Kurdjumov-Sachs orientation relationship between the α phase and the γ phase, we define the growth directions of the α phase with the preferential growth orientation θ_0. Other interfacial parameters and physical values in this study are given as follows [5]: the average interfacial energy is σ = 1.0 J/m^2, the mode number of interfacial anisotropy is k = 2 and the interfacial thickness is δ = 93.7 nm. Figures 1 (b) and (c) illustrate the computational models for the FEH analysis. x_i and y_i (i = 1, 2) indicate the coordinates in the macro- and microscopic regions, respectively. As shown in Fig. 1 (b), the microstructure in the Fe-C alloy is represented by the periodic arrangement of hexagonal unit-cells and the periodic boundary condition is employed for the unit-cells [12]. The unit-cell is modeled from the PF simulations. In order to study the deformation behavior under tensile deformation, a uniform tensile deformation is applied to the Fe-C alloy at a strain rate of $\dot{E} = 10^{-3}$ /s.

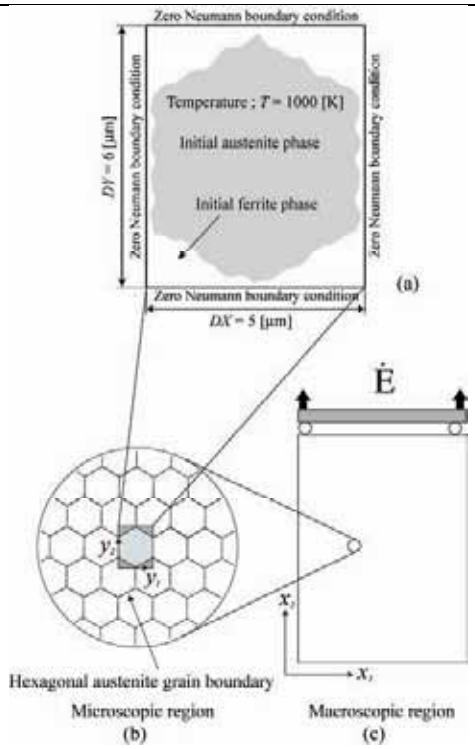

Figure 1. Computational models and initial conditions for (a) PF simulation and FEH analysis in (b) micro- and (c) macroscopic regions.

5 Results and Discussion

5.1 Microstructural evolution during isothermal γ / α transformation

The evolution of the α phase due to the isothermal γ/α transformation is simulated. Here, we investigate the effects of interfacial anisotropy on the morphological change of the α phase.

Figure 2 shows the distribution of carbon concentration during the evolution of the α phase for ξ = 0.2. We can observe that the initial α/γ interface migrates with carbon diffusion to the austenite matrix. It is also found that low interfacial anisotropy induces the growth of the α_A. We note that the interfacial migration behaviour with carbon diffusion and the build-up of carbon concentration in front of the moving interface can be simulated by the PF method.

On the other hand, as shown in Fig.3, many Widmanstätten ferrite (α_w) plates nucleate and grow from the initial α_A in the case of the higher strength of anisotropy ξ = 0.5. Here, the preferential growth direction of the α phase, θ_0, is the same as the case of Fig.2. From this result, the α_w growth mechanism can be described as follows: (i) the initial α_w tips are nucleated on the interface of the α_A, as shown in Fig.3 (a). In particular, the convex part of the initial interface is the preferential growth part of α_w. (ii) Some initial α_w tips coalesce into neighbouring tips and grow competitively toward the α_w plate. (iii) After the coalescence, each α_w plate evolves at a constant rate. Additionally, the rate of α/γ interface migration during the growth of α_w plates is clearly faster than that of α_A formation. Note that the simulated growth mechanism of the α_w plates is similar to the diffusional ledge-wise growth mechanism [13]. Furthermore, the experimentally observed morphology of the α_w plate, such as the parallel broad sides and the fine shape of the tip, can be simulated by employing the gradient energy coefficient [14].

Figure 4 shows the evolution of the α_w plate for ξ = 0.4. We define θ_0 so as to simulate the growth of the α_w plate from one part of the interface on the α_A. It is clearly observed that the coarse-grain α_w plate is so large that it grows across the γ grain. The growth rate of α_w plates decreases with decreasing the strength of anisotropy.

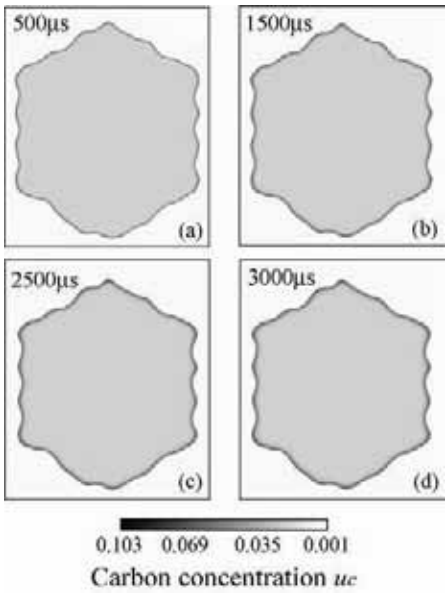

Figure 2. Growth of allotriomorph ferrite for strength of anisotropy ξ = 0.2.

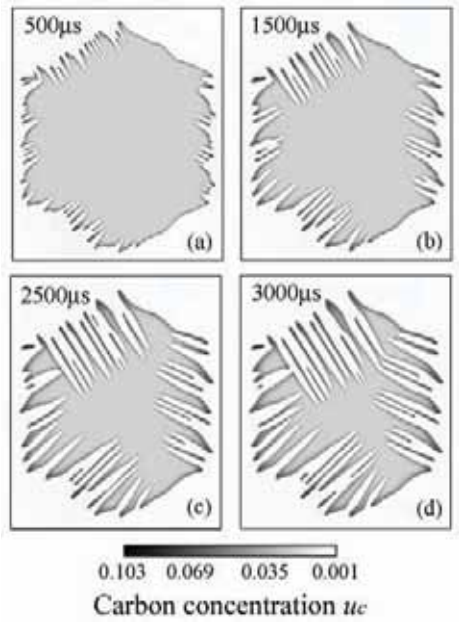

Figure 3. Growth of Widmanstätten ferrite for strength of anisotropy ξ = 0.5.

5.2 Unit-cell models for FEH analysis

Figure 5 illustrates the unit-cell models with different morphologies and volume fractions of the α phase. The total numbers of nodes and crossed-triangle elements of the unit-cell are also indicated. The unit-cell model is produced by employing the digital–image based modelling method using the image-data obtained by the PF simulation [15]. Here, (a) PFA-26, (b) PFW-57 and (c) PFL-54 correspond to the microstructures shown in Fig.2 (d) (α_A structure), Fig.3 (d) (fine-grained α_w structure) and Fig.4 (d) (coarse-grained α_w structure), respectively. As mentioned above, we consider the Fe-C alloy as the ferrite-pearlite two-phase steel. Therefore, we assume that the untransformed austenite phase in the PF simulation decomposes into pearlite during the subsequent cooling process. The distribution of the constituent phase is determined using the profile of the phase field $\phi = 0.5$, and the physical parameters are defined for each crossed-triangle finite element. The white and black areas in the unit-cell correspond to the pearlite and the α phases, respectively. The mechanical property of the pearlite depends on the ferrite-cementite lamellar spacing. However, in this study, we assume that the pearlite has an uniform structure. Accordingly, the initial yield stress of the constituent phase is σ_y = 409 MPa for the α phase and σ_y = 490 MPa for the pearlite. The Young's modulus of the Fe-C alloy is E = 206 GPa and the Poisson's ratio is $\nu = 0.3$ [16].

5.3 Effects of morphology of ferrite phase on mechanical properties of Fe-C alloy

We perform FEH analysis using the unit-cell models to clarify the effects of the morphological change of the microstructure on

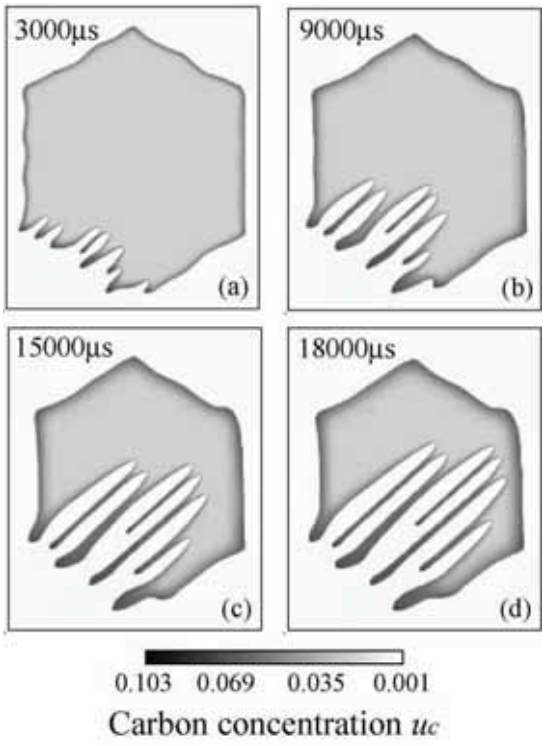

Figure 4. Growth of Widmanstätten ferrite across the pior-austenite grain for strength of anisotropy $\xi = 0.4$.

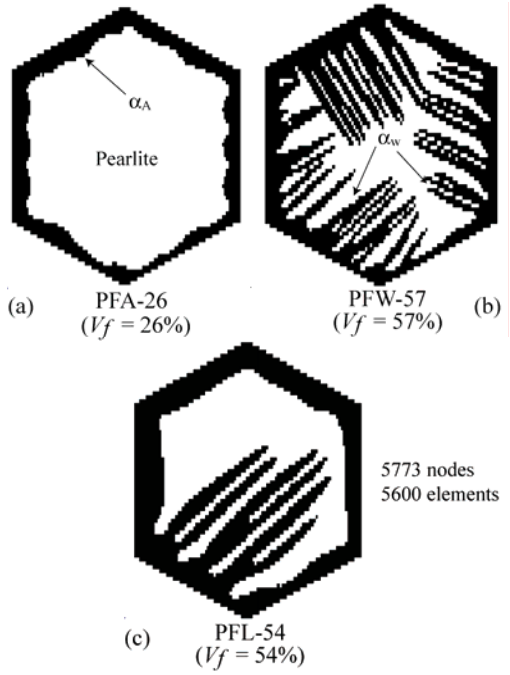

Figure 5. Unit-cell models with different morphologies and volume fractions of ferrite phase: (a) allotriomorph ferrite, (b) fine- and (c) coarse-grained Widmanstätten ferrite plates.

the mechanical properties of the Fe-C alloy.

Figure 6 illustrates the macroscopic nominal stress-nominal strain relationships for the Fe-C alloy containing different simulated microstructures. Although the strain hardening behaviour of all alloys is similar, we can observe that the maximum stress decreases with increasing volume fraction of the softer α phase. This volume-fraction-dependent behaviour is similar to that found in the experimental study [16]. However, the increase the yield stress and the strain hardening properties due to the formation of a fine-grained α structure cannot be simulated, because we do not consider the grain-size effect in this analysis. In a future study, we will simulate the size-dependent deformation behaviour using crystal plasticity theory [17].

Figure 7 shows the evolution of the microscale equivalent plastic strain in the unit-cell for (a) PFA-26, (b) PFW-57 and (c) PFL-54, for the macroscopic nominal strains E_n =0.1, 0.2 and 0.3. As shown in the figure, it is clear that the plastic deformation distribution is rather inhomogeneous and depends on the morphology of the α phase. In the case that the α phase exhibits an allotriomorphic structure, as for PFA-26, the plastic strain tends to be concentrated on the α_A formed along the prior-austenite grain boundary. Therefore, if the α_A phase grows in a coarse-grained morphology, the α_A phase may play a key role

in the fracture behavior of the Fe-C alloy, as reported in the literatures [18, 19].

For PFW-57, on the other hand, we can observe that the α_w plates in the unit-cell mainly plastically deform. That is, the plastic strain is not localized on the grain boundary, but is distributed almost uniformly in the unit-cell along the α_w plates. Furthermore, the magnitude of plastic strain in the unit-cell for PFW-57 is lower than that for PFA-26.

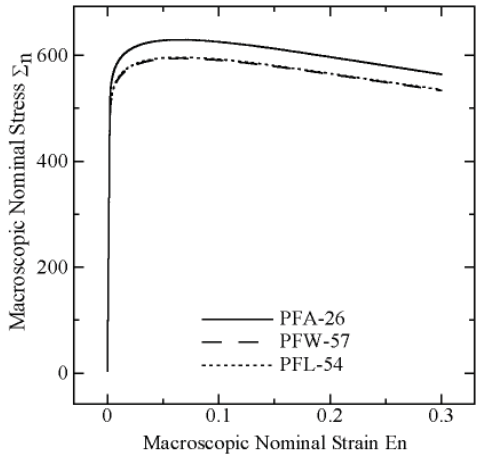

Figure 6. Macroscopic nominal stress vs nominal strain relationship.

From these results, we conclude that the strain redistribution due to the formation of fine-grained α_w plates causes the increase in toughness, as shown in the experimental studies [18]. On the other hand, in PFL-54, when the coarse-grained α_w structure is present in parallel formations across the austenite grain and the spacing between the plates is large, the plastic strain is predominantly distributed on the plates even though the α phase exhibits the α_w structure.

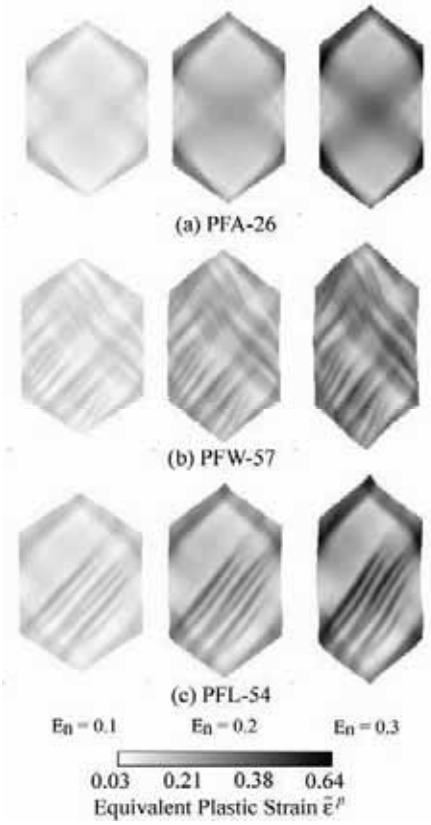

Figure 7. Distribution of equivalent plastic strain in the unit-cell.

Acknowledgments

Financially supported from the Ministry of Education, Culture, Sports, Science and Technology of Japan though Grand-in-Aid for Scientific Research (B), 18360061, 2007 and for JSPS Research Fellow is acknowledged.

References

[1] Krauss, G. and Thompson, S. W., (1995), Ferritic Microstructures in Continuously Cooled Low- and Ultralow-carbon steels, *ISIJ Int.*, 35, 937-945.

[2] Kobayashi, R., (1993), Modeling and Numerical Simulations of Dendritic Crystal Growth, *Phys. D*, 63, 410-423.

[3] Grudes, J. M. and Kikuchi, N., (1990), Preprocessing and Postprocessing for Materials Based on the Homogenization Method with Adaptive Finite Element Method, *Comp. Meths. Appl. Mech. Engn.*, 83, 143-198.

[4] Higa, Y. and Tomita, Y., (1999), Computational Prediction of Mechanical Properties of Nickel-Based Superalloy with Gamma Prime Phase Precipitates, *Advances Materials and Modeling of Mechanical Behaviour*, Vol. III, 1061-1066.

[5] Yamanaka, A. Takaki, T. and Tomita, Y., (2006), Phase-field Simulation of Austenite to Ferrite transformation and Widmanstätten ferrite formation in Fe-C Alloy, *Mater. Trans. JIM*, 47, 2725-2731.

[6] Gustafson, P., (1985), Thermodynamic Evaluation of the Fe-C System, *Scand. J. Metall.*, 14, 259-267.

[7] Takaki, T. Hasebe, T. and Tomita, Y., (2006), Two-dimensional Phase-field Simulation of Self-assembled Quantum Dot Formation, *J. Crys. Grow.*, 287, 295-299.

[8] Hillert, M., (1975), Diffusion and Interface Control of Reaction in Alloys, *Metall. Trans. A*, 6, 1350-1355.

[9] Ågren, J., (1986), A Revised Expression for the Diffusivity of Carbon in Binary Fe-C Austenite, *Script. Mater.*, 20, 1507-1510.

[10] Ågren, J., (1982), Computer Simulation of the Austenite/Ferrite Diffusional Transformations in Low Alloyed Steels, *Acta Metall.*, 30, 841-851.

[11] Tomita, Y., (1990), *Numerical Elasto-Plastic Mechanics*, YOKENDO Ltd.

[12] Ohno, T., Matsuda, T. and Wu, X. (2001), A Homogenization Theory for Elastic–viscoplastic Composites with Point Symmetry of Internal Distributions, *Int. J. Solids. Struct.*, 38, 2867-2878.

[13] Enomoto, M., (1994), Thermodynamics and Kinetics of the Formation of Widmanstätten Ferrite Plates in Ferrous Alloy, *Metall. Mater. Trans. A.*, 25A, 1947-1955.

[14] Yang, Z-G.. Wang, J-J., Li, C-M., Fang, H-S. and Zheng, Y-K., (1998), Ledges in Widmanstätten Ferrite Observed by Scanning Tunneling Microscopy, *J. Mater. Charac.*, 17, 331-333.

[15] Terada, K. and Kikuchi, N., (1998), Microstructural Modeling Technique for Homogenization Analysis Using Digital Images, *Trans. JSMS*, 64, 170-177.

[16] Ishikawa, N. Parks, D. M., Socrate, S. and Kurihara, M. (2000), Micromechanical Modeling of Ferrite-Pearlite Steels Using Finite Element Unit Cell Models, *ISIJ Int.,* 40, 1170-1179.

[17] Higa, Y. and Tomita, Y., (2003), Computational Simulation of Characteristic Length Dependent Behavior of Polycrystalline Metals, *Trans. JSMS*, 69, 23-29.

[18] Bodnar, R. L. and Hansen, S. S., (1994), Effects of Widmanstätten Ferrite on the Mechanical Properties of a 0.2 Pct C-0.7 Pct Mn Steel, *Metall. Mater. Trans. A*, 25A, 763-773.

[19] Gulyaev, A. P. and Guzovskaya, M. A., (1977), Resistance to Fracture of Weldable Carbon Structural Steel with Ferrite-Pearlite and Widmanstätten Structures, *Met. Sci. Heat Treat.*, 19, 1020-1024.